Circularly Polarized High Gain Leaky-Wave Antenna for CubeSat Communication

***Q*: What is the problem being addressed by the manuscript and why is it important to the Antennas & Propagation community? (limited to 100 words).**

A: The proposed compact planar LWA and its array provide promising CP radiation in terms of ARs, bandwidth, polarization flexibility, impedance matching, efficiency and gain, which reveals great potential for applications in satellite communication systems that demanding low profile, light weight, dual CPs and high directivity.

***Q*: What is the novelty of your work over the existing work? (limited to 100 words).**

A: In this paper, both left-handed (LH) and right-handed (RH) CPs are achieved in a wide beam steering range backwardly or forwardly. The LHCP/RHCP steering beams ranges from −51 °to 0 °or from 51 °to 0 °in the elevation when the frequency varies from 27.4 to 37.3 GHz. In the 30% frequency band, the axial ratios (ARs) on the main beams are all less than 3 dB demonstrating the broadband CP characteristic.

***Q*: Provide up to three references, published or under review, (journal papers, conference papers, technical reports, etc.) done by the authors/coauthors that are closest to the present work. Upload them as supporting documents if they are under review or not available in the public domain. Enter "N.A." if it is not applicable.**

A: [25] J. Wang, Y. Geng, C. Zhang and X. Huo, "Radiation characteristic of the periodic leaky wave structure and its application to leaky wave antenna design," 2015 Asia-Pacific Microwave Conference (APMC), Nanjing, 2015.

[26] X. Li, J. Wang, Z. Li, Y. Li, M. Chen and Z. Zhang, "Dual-Beam Leaky-Wave Antenna Array With Capability of Fixed-Frequency Beam Switching," IEEE Access, vol. 8, pp. 28155-28163, 2020.

[27] X. Li, J. Wang, Z. Li, Y. Li, Y. Geng, M. Chen and Z. Zhang, " Leaky-wave Antenna Arrays for Flexible Dual-beam Switching," IEEE Trans. Antennas Propag, Early access, 2021.

***Q*: Provide up to three references (journal papers, conference papers, technical reports, etc.) done by other authors that are most important to the present work. Enter "N.A." if it is not applicable.**

A: [42]Y. J. Cheng, W. Hong, and K. Wu, "Millimeter-wave half mode substrate integrated waveguide frequency scanning antenna with quadri-polarization," *IEEE Trans. Antennas Propag.*, vol. 58, no. 6, pp. 1848–1855, 2010.

[43]Y. Dong and T. Itoh, "Substrate integrated composite right-/left-handed leaky-wave structure for polarization-flexible antenna application," *IEEE Trans. Antennas Propag*., vol. 60, no. 2, pp. 760–771, 2012.

[44]A. Sarkar, S. Mukherjee, A. Sharma, A. Biswas and M. Jaleel Akhtar, "SIW-Based Quad-Beam Leaky-Wave Antenna With Polarization Diversity for Four-Quadrant Scanning Applications," *IEEE Trans. Antennas Propag.*, vol. 66, no. 8, pp. 3918-3925, Aug. 2018.

Circularly Polarized High Gain Leaky-Wave Antenna for CubeSat Communication

Xiaowen Li, *Student Member*, *IEEE*, Junhong Wang, *Senior Member*, *IEEE*, George Goussetis, *Senior Member*, *IEEE*, Lei Wang, *Senior Member*, *IEEE*

***Abstract*—In this work, a novel planar leaky-wave antenna and its array are proposed and presented for CubeSat communication applications. Utilizing the substrate integrated waveguide (SIW) technology, the proposed LWA is implemented by etching periodic fan-shape slots on the top of an SIW. These novel fan-shape slots exhibit extraordinary circularly polarized (CP) radiation in high efficiency over a wide frequency band. Moreover, by switching the excitation ports, both left-handed (LH) and right-handed (RH) CPs are achieved in a wide beam steering range backwardly or forwardly. An SIW LWA prototype has been designed and tested with validate LHCP/RHCP steering beams ranging from −51 ° to 0 ° or from 51 ° to 0 ° in the elevation when the frequency varies from 27.4 to 37.3 GHz. In the 30% frequency band, the axial ratios (ARs) on the main beams are all less than 3 dB demonstrating the broadband CP characteristic. In this one-dimensional LWA, the realized gain varies from 12.4 to 17.9 dBi. However, it requires higher gain and a fixed beam but narrow bandwidth in some applications like CubeSats. Hence, a conformal LWA array is further introduced by combining the CP radiation of two LWAs deployed in two perpendicular surfaces of a 1U CubeSat. Fed by an elaborated vertical transition, the conformal array is designed at 28 GHz with a high directive sum beam along the diagonal direction, requiring each LWA to radiate at ±45 °. As a result, the total gain is enhanced from 14.4 to 16.6 dBi with an AR of 1.8 dB and a side-lobe level of −17.1 dB. The proposed compact planar LWA and its array provide promising CP radiation in terms of ARs, bandwidth, polarization flexibility, impedance matching, efficiency and gain, which reveals great potential for applications in satellite communication systems that demanding low profile, light weight, dual CPs and high directivity.**

***Index Terms*—Circular polarization, conformal array, CubeSat, leaky-wave antenna (LWA), substrate integrated waveguide (SIW).**

I. Introduction

CUBESAT has been proposed as a promising solution for advanced Low-Earth Orbit missions, and becomes the most popular nanosatellite standard [1]-[3]. As a typical small satellite, the size of CubeSat is a multiple of one cubic unit (1U) of 10×10×10 cm3. Generally, the weight of CubeSat composed of 0.25-27U ranges from 0.2 to 20 kg as 1U CubeSat weighs less than 1.33 kg. Due to its structural and physical features, the CubeSats requires a high-quality and light-weight communication system, which highly depends on key components like antennas.

CubeSat antennas, in terms of the structural and operation mechanism, can be divided into two categories: space deployment antennas and planar antennas. The space deployment antennas are bulky and heavy in structure, bringing challenges in the integration and radiation efficiency. Therefore, most space deployment antennas are designed to be foldable or furlable and deployable. During the launch, they are mechanically packed into a small storage space of the CubeSat, and then deployed outside the CubeSat for communication. Various innovative techniques and theories have been put forward in the deployment schemes [4]-[13], including a mesh offset modeling technique, spatial-mapping origami theory, etc. These design schemes successfully overcome the challenges caused by large-size structures, but their limitation is also obvious, that is, they increase the design complexity and cost. The above limitation can be directly avoided using planar antennas, because the low-profile characteristic of planar antennas makes it well conformal with CubeSat or its solar panels. As CubeSats can be networked to form satellites constellations or swarms, the functions of self-beam steering with improved directivity, higher gain and CP are preferred by CubeSats to establish communication links between them [23][24]. Planar antennas of CubeSat [14]-[22] usually adopt microstrip structures, such as patch antennas and dipoles that have radiation patterns with wide beamwidth and weak directivity. Furthermore, according to the comparison between all types of planar antennas given in survey results [23], few planar antennas (1/32) can realize self-steering and circular polarization (CP) at the same time [24]. In this respect, the leaky-wave antenna (LWAs) based on a substrate integrated waveguide (SIW), exhibits natural advantages for the CubeSats, such as small profile, high directivity, frequency beam scanning [25, 26, 27]. Therefore, this paper mainly focuses on the study of CubeSat LWAs, especially the realization of another two characteristics needed for the CubeSat communication, namely CP and high gain.

This work was supported by a scholarship of China Scholarship Council. (Corresponding author: Xiaowen Li; Lei Wang)

X. Li is with the Key Laboratory of All Optical Network & Advanced Telecommunication Network of the Ministry of Education, China, and the Institute of Lightwave Technology, Beijing Jiaotong University, Beijing 100044, China, and also with the Institute of Sensors, Signals and Systems, Heriot-Watt University, Edinburgh EH14 4AS, United Kingdom (e-mail: 17111055@bjtu.edu.cn).

J. Wang is with the Key Laboratory of All Optical Network & Advanced Telecommunication Network of the Ministry of Education, China, and the Institute of Lightwave Technology, Beijing Jiaotong University, Beijing 100044, China (e-mail: wangjunh@bjtu.edu.cn).

G. Goussetis and L. Wang are with the Institute of Sensors, Signals and Systems, Heriot-Watt University, Edinburgh EH14 4AS, United Kingdom (e-mail: lei.wang@hw.ac.uk, g.goussetis@hw.ac.uk).

As we know, circularly polarized antennas offer the polarization matching and flexibility desired by satellite communication, which also suppress multipath interferences. For realizing the CP property, most SIW LWAs design their aperture slots to construct two perpendicular electric components with equal amplitude and 90-degrees phase difference. There are many types of CP slots with different branch shapes in press. In [28], radiation unit of T-shaped interdigital slot is presented, based on which composite right/left-handed (CRLH) transmission line feature and CP characteristic are obtained. As validated by measurement of phototype, it achieves a CP-featured beam scanning from −19 to 84 degrees over a frequency range of 7.35 -10.14 GHz. Such T-shaped slot or slot pair loaded LWAs with CP characteristic are also provided in [29]-[35]. In [36], a benzene-ring-shaped slot-loaded LWA with partially reflecting wall vias is investigated, which realizes a continuous CP beam steering range of 97.1 degrees when the frequency varies from 9.35 to 11.75 GHz. In addition, the CP properties of LWA are also implemented by employing H or S-shaped slots [37, 38], cross or ramp slot [39, 40], etc. Different from the above work, an even-odd analysis method is proposed in [41] to design an inclined slot group with 45-degrees linear polarization (LP), and by combining two LWAs with 45-degrees LP through a 3 dB coupler, CP operation is obtained. The scan range of this CP LWA is from -30 to 22 degrees in a frequency band of 9.6 - 10.8 GHz. Beyond the above CP realization, [42]-[44] also focus on the characteristic of polarization flexible (pol-flexible) CP of SIW LWAs. They use two transversely distributed LWA units with the 45-degrees inclined slots, interdigital or doubly arranged slots for generating two E-components with comparable amplitudes. Then, by adopting a multiport directional coupler or a rat race coupler at the end of the two-channel array, 90 or −90-degrees phase difference between the two individually controlled LWAs is realized and selected, making CP generation and flexibility come true.

In this paper, we aim to realize the CP property and CP flexibility of LWA by designing a novel slot in a fan shape. Without introducing composite radiation slot or extra coupler, this design owns the advantages of compact structure and simple design procedures. In the full-wave simulation, it is proved that the designed pol-flexible CP LWA is able to scan from -51° to 51° by varying the frequency between 27.4 and 37.3 GHz. Moreover, another advantage of the proposed LWA is that it overcomes the open stopband itself thanks to the periodic asymmetric slots. Furthermore, by using spatial pattern superposition theory, the sub radiation patterns of two proposed SIW LWA are combined into a sum beam with high gain. In this design process, in addition to maintaining the good conformal structure and CP characteristic, we also obey the principle of no introduction of extra devices and design complexity. Two independent SIW channel are simultaneously excited by feeding one of them and coupling to the other one through an interactive coupling aperture. The paper is organized as follows: In Section II, the basic scenario of this work and its CP sub pattern superposition method are given. In Section III, the design process of CP LWA element with fan-shaped slots and its simulated results are shown. Then, the realization of conformal high gain CubeSat array is depicted in Section IV. Measured results of single LWA element and LWA array with sum beam are shown in Section V. Finally, conclusions are drawn in Section VI.

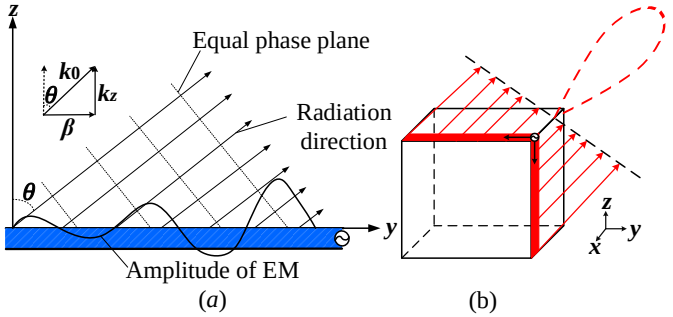

Fig. 1. Illustration of the proposed design method, (a) Radiation mechanism of leaky-wave antenna; (b) Sum beam with high gain combined by sub patterns of two perpendicularly arranged LWA.

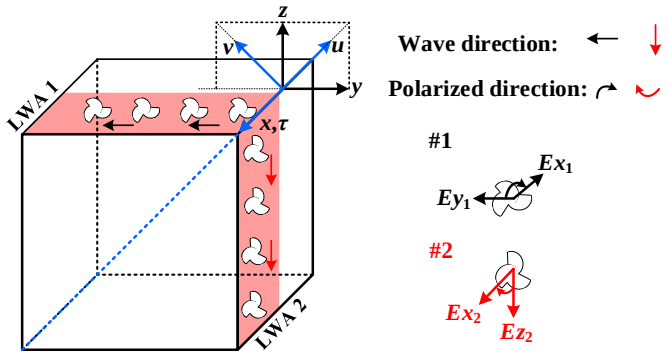

Fig. 2. Schematic diagram of pattern superposition analysis.

II. Main Analysis

A. Basic Scenario

Fig. 1 illustrates the proposed scenario of conformal high gain CubeSat SIW LWA. As shown in Fig. 1 (a), SIW LWA is basically a waveguide structure that possesses a mechanism that permits it to leak power all along its length. The aperture field of an LWA has an exponential decay, and this design is based on an SIW LWA operating in the −1th spatial harmonic mode with backward radiation of 45 degrees. By skillfully utilizing the low-profile feature of the SIW LWA, we arrange two above SIW LWAs perpendicularly at one corner of a 1U CubeSat depicted in Fig. 1 (b), and then their leaky wave hopefully reach the equal phase plane together. As they have identical structures, their leaky amplitudes are equal. If their beams can be superposed effectively, a sum beam with higher gain, represented by the red dashed pattern pointing at the diagonal direction in Fig. 1 (b), can be obtained. With this expectation, we will discuss the superposition mechanism of sub patterns with CP property in Section II. B.

B. CP Superposition

As introduced in last section, we aim to design a fan-shaped slot that owns curl property to achieve a pol-flexible CP LWA. Fig. 2 shows a sketch of the designed conformal LWA of

CubeSat, in which several fan-shaped slots are drawn to represent the periodic slots in practice. Here, we name the upper LWA on the *xoy* plane as LWA 1 and the lower LWA on the *xoz* plane as LWA 2. As we know, CP property generates two electric components with an equal amplitude and a phase difference of 90 degrees. It is assumed that the CP properties of LWA 1 and LWA 2 are ideal LHCP, and the phase of electric component in wave-propagating direction is 90 degrees ahead that of the other one, according to which the aperture electric vectors of LWA 1 and LWA 2, namely $\boldsymbol{E}_{x1,2}$, $\boldsymbol{E}_{y1,2}$ and $\boldsymbol{E}_{z1,2}$, are also given in Fig. 2, and distinguished by subscripts 1 and 2 for two different LWA elements.

For LWA 1, there are two electric components on its aperture: $\boldsymbol{E}_{x1}$, $\boldsymbol{E}_{y1}$ of which $|\boldsymbol{E}_{x1}|$ is equal to $|\boldsymbol{E}_{y1}|$ and the phase of $\boldsymbol{E}_{y1}$ is 90 degrees ahead of that of $\boldsymbol{E}_{x1}$ as depicted in (1) and (2).

$$\boldsymbol{E}_{x1} = -\hat{\boldsymbol{e}}_x|\boldsymbol{E}_{x1}|e^{j0}, \tag{1}$$

$$\boldsymbol{E}_{y1} = -\hat{\boldsymbol{e}}_y|\boldsymbol{E}_{y1}|e^{-j90}, \tag{2}$$

where $\hat{\boldsymbol{e}}_x$ and $\hat{\boldsymbol{e}}_y$ are the unit vectors of $\boldsymbol{x}$ and $\boldsymbol{y}$ direction. Similarly, the expressions of the aperture electric components of LWA 2 are:

$$\boldsymbol{E}_{x2} = \hat{\boldsymbol{e}}_x|\boldsymbol{E}_{x2}|e^{j0}, \tag{3}$$

$$\boldsymbol{E}_{z2} = -\hat{\boldsymbol{e}}_z|\boldsymbol{E}_{z2}|e^{-j90}, \tag{4}$$

where $\hat{\boldsymbol{e}}_z$ is the unit vector of $\boldsymbol{z}$ direction and $|\boldsymbol{E}_{x2}|$ is equal to $|\boldsymbol{E}_{z2}|$.

1) In Phase Superposition

Since LWA 1 and LWA 2 are identical, they can have consistent strength E_0 of electric components. Thus, the amplitude relationship between above electric components can be concluded as:

$$|\boldsymbol{E}_{x1}| = |\boldsymbol{E}_{x2}| = |\boldsymbol{E}_{y1}| = |\boldsymbol{E}_{z2}| = E_0. \tag{5}$$

By adding the electric components of LWA 1 and LWA 2 together, the vector expression of sum electric field (6) can be obtained.

$$\boldsymbol{E} = -\hat{\boldsymbol{e}}_y|\boldsymbol{E}_{y1}|e^{-j90} - \hat{\boldsymbol{e}}_z|\boldsymbol{E}_{z2}|e^{-j90} = -(\hat{\boldsymbol{e}}_y + \hat{\boldsymbol{e}}_z)E_0e^{-j90}. \tag{6}$$

In order to clarify the direction of $\boldsymbol{E}$, as depicted in Fig. 2, we define a new coordinate system with three mutually vertical spatial vector variables $\boldsymbol{u}$, $\boldsymbol{v}$, $\boldsymbol{\tau}$. It can be observed that the relationships between the unit vectors in $\boldsymbol{x}$, $\boldsymbol{y}$, $\boldsymbol{z}$ and $\boldsymbol{u}$, $\boldsymbol{v}$, $\boldsymbol{\tau}$ directions are:

$$\begin{cases} \hat{\boldsymbol{e}}_u = \dfrac{\sqrt{2}}{2}(\hat{\boldsymbol{e}}_y + \hat{\boldsymbol{e}}_z) \\ \hat{\boldsymbol{e}}_v = \dfrac{\sqrt{2}}{2}(-\hat{\boldsymbol{e}}_y + \hat{\boldsymbol{e}}_z) \\ \hat{\boldsymbol{e}}_\tau = \hat{\boldsymbol{e}}_x \end{cases}. \tag{7}$$

Combining formula (5) and (7), sum vector of formula (6) can be redefined by the $\boldsymbol{u}$, $\boldsymbol{v}$, $\boldsymbol{\tau}$ coordinate system as:

$$\boldsymbol{E} = -\hat{\boldsymbol{e}}_u|\boldsymbol{E}_u|e^{-j90} = -\hat{\boldsymbol{e}}_u\sqrt{2}E_0e^{-j90}, \tag{8}$$

where $|\boldsymbol{E}_u|$ is equal to $\sqrt{2}E_0$.

We can see that $\boldsymbol{E}$, the sum electric vector of LWA 1 and LWA 2, is a vector along the propagation direction of $\hat{\boldsymbol{e}}_u$. Moreover, using the above analysis method, we explored the superposition cases when the excitation sources of LWA 1 and LWA 2 are with a certain phase difference and found that the $\boldsymbol{E}$ has two orthogonal components with a phase difference of 90 degrees constituting circular polarization characteristic when the phase difference is 180 degrees. The detailed proof processes are as follows.

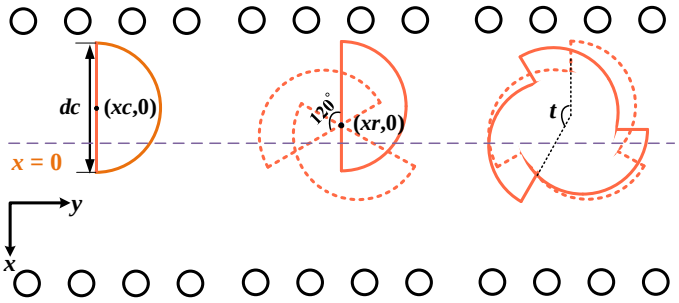

Fig. 3. The proposed fan-shaped slot with curl characteristic at y=0. (a) Shape of semicircle as the fan branch. (b) Union and forming of the fan-shaped slot. (c) Self rotation of the fan-shaped slot.

2) Out of Phase Superposition

With the excitation phase difference of 180 degrees, formula (3) and (4) are updated to:

$$\boldsymbol{E}_{x2} = \hat{\boldsymbol{e}}_xE_0e^{j180}, \tag{9}$$

$$\boldsymbol{E}_{z2} = -\hat{\boldsymbol{e}}_zE_0e^{j90}. \tag{10}$$

Now, the sum vector $\boldsymbol{E}$ is reorganized to:

$$\begin{aligned} \boldsymbol{E} &= -2\hat{\boldsymbol{e}}_x|\boldsymbol{E}_{x1}| - (-\hat{\boldsymbol{e}}_y + \hat{\boldsymbol{e}}_z)|\boldsymbol{E}_{y1}|e^{-j90} \\ &= -2\hat{\boldsymbol{e}}_\tau|\boldsymbol{E}_\tau| - \hat{\boldsymbol{e}}_v|\boldsymbol{E}_v|e^{-j90} \\ &= -\sqrt{2}E_0(\sqrt{2}\hat{\boldsymbol{e}}_\tau + \hat{\boldsymbol{e}}_ve^{-j90}), \end{aligned} \tag{11}$$

where $|\boldsymbol{E}_\tau| = |\boldsymbol{E}_{x1}|$, $|\boldsymbol{E}_v| = \sqrt{2}|\boldsymbol{E}_{y1}|$. Different from the $\boldsymbol{E}$ obtained in (8), the two components of $\boldsymbol{E}$ here are vertical to the propagation direction of $\hat{\boldsymbol{e}}_u$, which conforms to the features of TEM wave. It can be seen that, the two field components of the $\boldsymbol{E}$ are orthogonal, their phase difference is 90 degrees, and the amplitude ratio is $\sqrt{2}$. Therefore, the superimposed electric field $\boldsymbol{E}$ satisfies the characteristics of elliptical polarization and has the possibility of generating circular polarization radiation pattern. In the process of array design, the farfield axial ratio is less than 3 dB to judge whether the array has circular polarization characteristics. With this theoretical basis, we designed a 180-phase difference feeding method of two-vertically arranged LWAs in Section IV, and with the help of full-wave simulation, the AR performance of sum pattern is fully considered.

III. Single LWA Design

With the help of the analysis in Section II, an SIW LWA radiating at −45 degrees with pol-flexible CP characteristic is designed in this section. Moreover, a systematic study and optimization of the proposed fan-shaped slots are given. Furthermore, the simulated radiation performances of the final LWA are shown and analyzed in the following.

A. Systematic Study of Fan-shaped Slots

The modeling process and final structure of the proposed fan-shaped slot are given in Fig. 3. There are four parameters studied in his section, namely *xc*, *dc*, *xr* and *t*. Among them, *xc* is the *x* coordinate value of the branch semicircle center

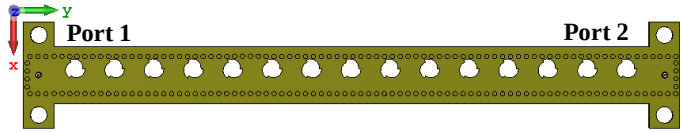

Fig. 4. The designed SIW LWA with periodic fan-shaped slot.

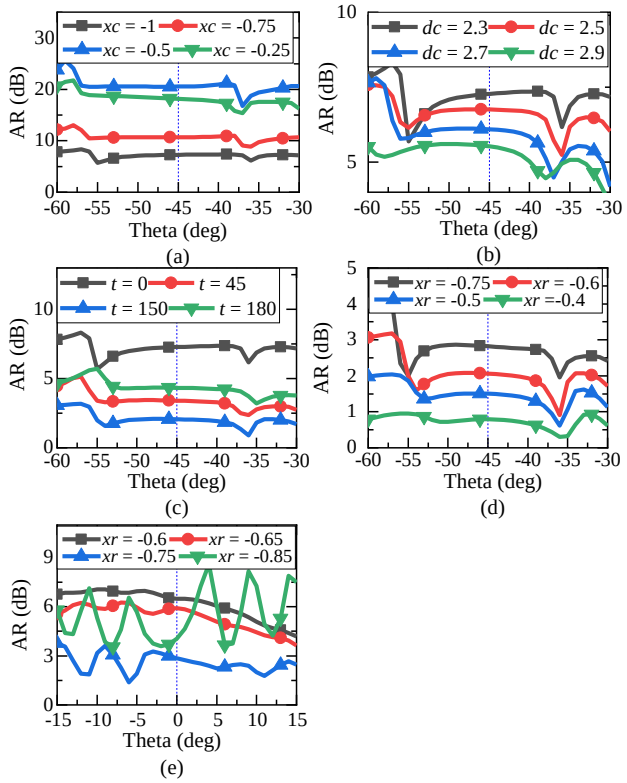

Fig. 5. The optimization process of AR performance. (a) different *xc* values (Unit: mm) for AR study at −45 °direction. (b) different *dc* values (Unit: mm) for AR study at −45 °direction. (c) different *t* values (Unit: degree) for AR study at −45 ° direction. (d) different *xr* values (Unit: mm) for AR study at −45 ° direction. (e) different *xr* values (Unit: mm) for AR study at 0 °direction.

depicted by in Fig. 3 (a), while the middle center line of SIW channel is $x = 0$ mm, and the diameter of the semicircle is *dc*. As shown in Fig. 3 (b), by rotating the semicircle by 120-degrees twice around the point (*xr*, 0) and uniting them together, a fan-shaped slot shown by the dotted line in Fig. 3 (c) can be obtained. Then, this fan-shaped slot is self-rotated by the angle of *t*, achieving the final fan-shaped slot illustrated by the solid line in Fig. 3 (c). For achieving a CP property, a parameter study of the fan-shaped slot is carried out through analyzing a SIW LWA, with a −45-degrees radiation pattern at 28 GHz, based on a Rogers RT5880 substrate with a thickness of 1.575 mm, a permittivity $\varepsilon_r = 2.2$ and a loss tangent of 0.0009. Fig. 4 shows the full structure of the proposed CP SIW LWA with a total length of 98 mm, including via walls with a width of 5.67 mm, fan-shaped slots with a period of 6.02 mm and two feeding ports, i.e., Port 1 and Port 2. In the CP optimization process of the LWA element, we choose Port 1 as the excitation port, and take the AR value of its farfield pattern less than 3 dB as a standard.

Fig. 5 gives the simulated AR values of the CP LWA with different structural parameters. The preliminary parameter values of *dc*, *t* and *xr* are set to 2.3 mm, 0 degree and −0.6 mm, respectively. Fig. 5 (a) gives the simulated AR curves of the LWA with different *xc* values of -0.25 mm, -0.5 mm, -0.75 mm and −1 mm. With the decrease of *xc*, the AR value at −45-degree direction decreases, so the *xc* is chosen to be −1 mm. Then, parameter *dc* is carefully tuned to observe its effect on the AR curve. Fig. 5 (b) depicts the AR results for four different *dc* of 2.3 mm, 2.5 mm, 2.7 mm and 2.9 mm. It is observed that when the value of *dc* increases, the AR value of −45-degree decreases as we expected. It should be noted that, when *dc* is larger than 2.7 mm, the etched slots will be too close to the side vias, resulting in fabrication difficulties. Therefore, even if the case of *dc* = 2.9 mm has better AR performance, we still choose *dc* = 2.7 mm. Next, the parameter *t* is set to one of the values of 0, 45, 150, 180 degrees, and the corresponding AR results are given in Fig. 5 (c). It can be seen that when *t* is 150 degrees, AR achieves less than 3 dB for the first time. Based on the above selected parameter values of *xc* = −1, *dc* =2.7 mm and *t* = 150 degrees, *xr* are further studied. As shown in Fig. 5 (d), AR performance is further improved as *xr* increases from −0.75 mm to −0.4 mm.

Due to the superpositions of reflective waves from slots distancing multiple times of half waveguide wavelength, it is difficult for most LWAs to realize broadside radiation, namely the open stopband (OSB) problem. As the designed fan-shaped slots owns an asymmetrical geometry, the reflective waves of slots will not be added in phase at the input port, allowing a broadside (0 degree) radiation. In this case, we also take the AR performance at 0-degree into consideration for realizing the targeted CP flexibility at the broadside direction. Fig. 5 (e) shows the AR performance of the LWA when *xr* gets an increasement of 0.05 mm from 0.6 mm. We can see that when *xr* is −0.75 mm, the AR at the broadside is approaching less than 3 dB. Thus, there is a tradeoff between the AR optimization between the radiation at −45 degrees and 0 degree. Finally, the parameter values of fan-shaped slots are *xc* = −1 mm, *dc* =2.7 mm, *t* = 150 degrees and *xr* = −0.75 mm are chosen, leading to the AR values of the final designed LWA at −45-degrees and 0-degree directions to be 2.82 dB and 2.85 dB.

B. Simulated Results of LWA Element

The simulated radiation performances of the proposed CP LWA element, including S-parameters, radiation efficiency, E-field, farfield patterns and ARs, are given in this section.

Fig. 6 shows the simulated S-parameters and dispersion diagram of the proposed CP LWA element. When the LWA is excited by either Port 1 or Port 2, the obtained S_{11} and S_{22} are all below −10 dB in a wide frequency band of 27.4 GHz – 37.3 GHz as shown in Fig. 6 (a). Besides, there is no OSB at 37.3 GHz that is the frequency verses the broadside radiation. As also depicted in this figure, due to the dispersion characteristic of the leaky-wave structure, the S_{21} and S_{12} deceases from – 4.7 dB to –17.4 dB with the increase of frequencies. Besides, the realization of OSB suppression comes from the asymmetrical geometry of the fan-shaped slots. Fig. 6 (b) illustrates the dispersion curves of an LWA element, in which the attenuation constant curves for *xc* = −0.25 mm, −0.75 mm, and −1 mm while the phase constant curve is plotted for *xc* = −1 mm. For *xc* = −0.25 mm and −0.75 mm, there is a significant ripple at 37.3 GHz in the αp curves representing the existence of OSB. However, the αp curve becomes flat for *xc* = −1 mm showing a complete elimination of the OSB. Meanwhile, in the case of *xc* = −1 mm, the βp curve is linear versus the frequency even at 37.3 GHz, further fulfilling the stopband elimination criteria.

This article has been accepted for publication in a future issue of this journal, but has not been fully edited. Content may change prior to final publication. Citation information: DOI 10.1109/TAP.2022.3167773, IEEE Transactions on Antennas and Propagation

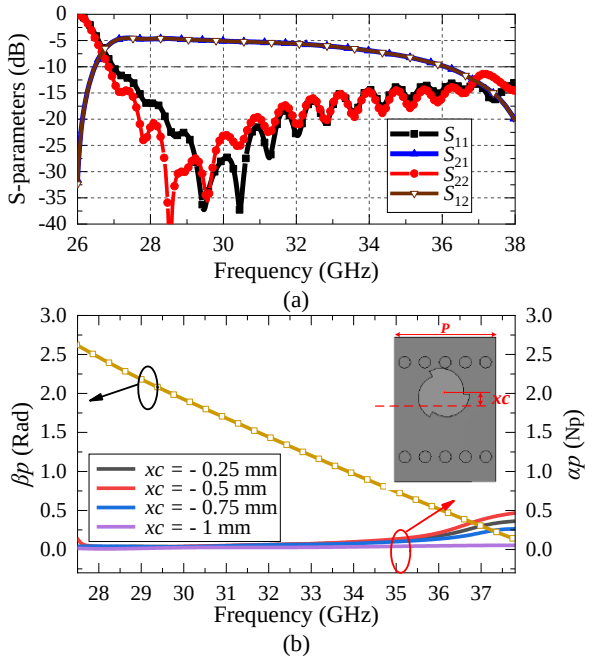

Fig. 6. (a) Simulated S-parameters of the proposed CP LWA element. (b)Simulated dispersion diagram of one unit.

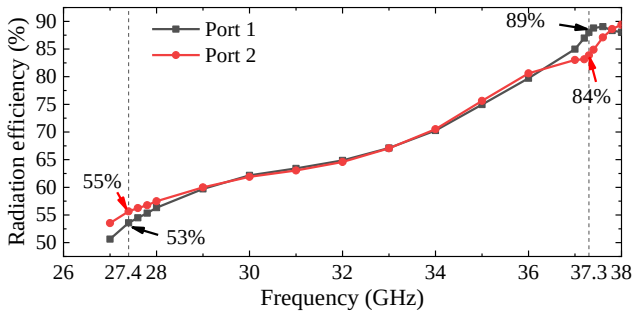

Fig. 7. Simulated radiation efficiencies of the proposed CP LWA element.

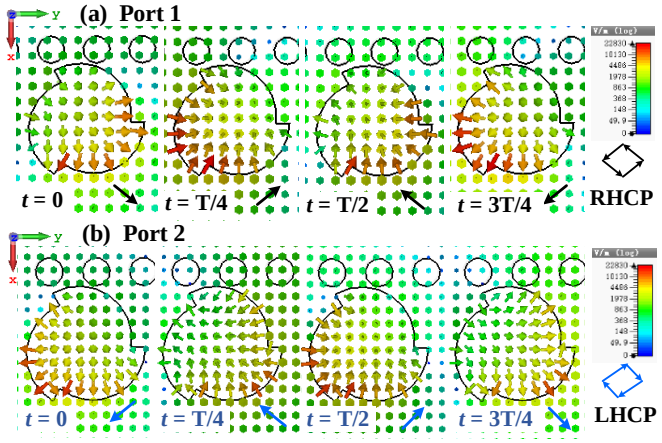

Fig. 8. Simulated E-field of the aperture slot in four-phase states at 28 GHz.

Fig. 7 gives the simulated radiation efficiency of the proposed single CP LWA. When the LWA is excited by Port 1, the radiation efficiency between 27.4 GHz – 37.3 GHz ranges from 53% to 89%. Similarly, an efficiency ranging in 55% - 84% is achieved when the Port 2 is excited. As mentioned earlier, since the leakage constant increases with the frequency,

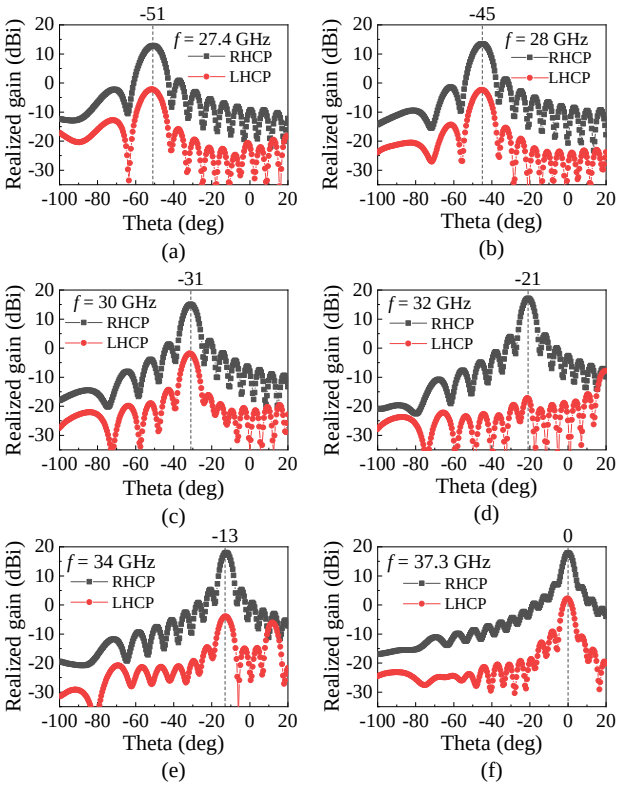

Fig. 9. Simulated radiation patterns of the proposed CP LWA element at different frequencies when Port 1 is excited. (a) 27.4 GHz. (b) 28 GHz. (c) 30 GHz. (d) 32 GHz. (e) 34 GHz. (f) 37.3 GHz.

the radiation efficiency also increases consequently in this process.

Fig. 8 depicts the simulated E-field on a slot aperture in four-phase states at 28 GHz. As shown in Fig. 8 (a), when Port 1 is excited, the E-field propagates counterclockwise in the *xoy* plane, which means that the corresponding CP state is left-handed along +*z* direction in this case. As depicted in Fig. 8 (b), when Port 2 is excited, the E-filed rotates clockwise in the *xoy* plane, leading to a right-handed CP radiation in +*z* direction. With the help of the E-field analysis, we can see that the proposed fan-shaped slot does make the CP flexibility of the LWA possible. And this method shows obvious advantages in structure minimization and simplification of design.

Fig. 9 and Fig. 10 show the simulated radiation patterns when the proposed CP LWA is excited by Port 1 and Port 2, respectively. As shown in Fig. 9, under the Port 1 excitation mode, the frequency-controlled beam scans from −51 degrees to 0 degree when the frequency *f* changes from 27.4 GHz to 37.3 GHz. The gain differences between the co-polarization (co-pol) pattern (RHCP) and the cross-polarization (cro-pol) pattern (LHCP) varies from 16.2 to 20.8 dB. Among them, the realized co-pol gains of *f* =27.4, 28, 30, 32, 34, 37.3 GHz are 12.4, 12.9, 14.5, 16.6, 17.5 and 17.9 dBi, respectively. As given in Fig. 10, the frequency beam scanning range is from 51 degrees to 0 degree as *f* varies from 27.4 GHz to 37.3 GHz in Port 2 mode. The gain difference between co-pol and cro-pol patterns ranges from 15.2 to 19.4 dB. And the co-pol gains of the above six frequencies are 12.6, 13, 14.5, 16.6, 17.5, 17.6

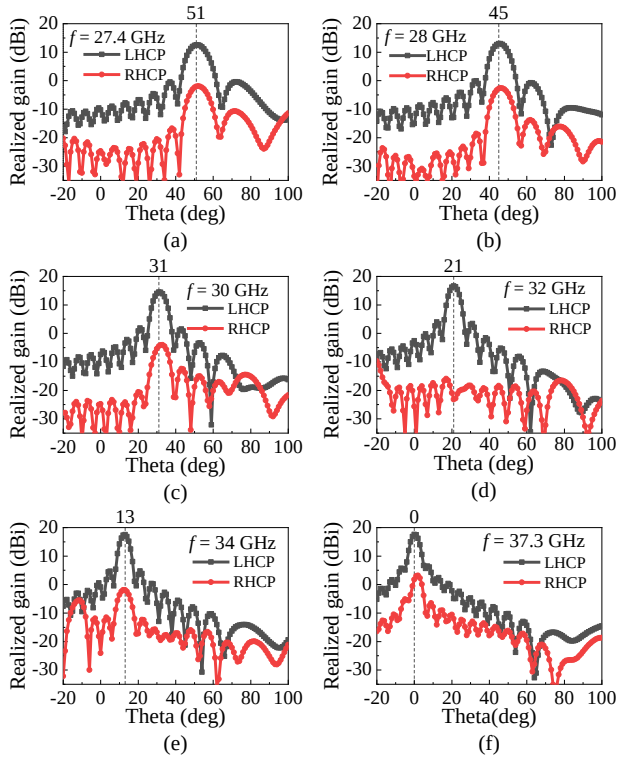

Fig. 10. Simulated radiation patterns of the proposed CP LWA element at different frequencies when Port 2 is excited. (a) 27.4 GHz. (b) 28 GHz. (c) 30 GHz. (d) 32 GHz. (e) 34 GHz. (f) 37.3 GHz

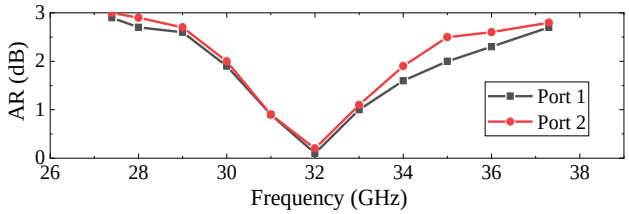

Fig. 11. Simulated AR values of the proposed CP LWA element.

TABLE I
COMPARISON BETWEEN THIS DESIGN AND OTHER POL-FLEXIBLE CP LWAS

Ref.	Size (λ_0)	CP band (GHz)	AR BW (%)	Angle range (deg)	Gain (dBi)
[42]	17 ×5.5	34 -37	8.5%	12~24	11.2-13.6
[43]	7.1×4.3	7.5-10	28.6%	−40~40	10.5-14.6
[44]	44×20	10.7-11.7	8.92%	16~76	9.2-12.1
This work	**10.6 ×1.7**	**27.4-37.3**	**31%**	**−51~ 0**	**12.4-17.9**
				0~51	**12.6-17.6**

dBi. We can see that the frequency-increased leakage constant results in an increasing gain versus frequencies. And as a slot with curve edges, the fan-shaped slot owns the curvilinear E-field that can be equivalent to two orthogonal ***E*** components for CP generation. When f = 32 GHz, the two orthogonal components are with more equal amplitudes, resulting in a lower CP cross-polarization level than those of other frequencies. Meanwhile, the well-maintained broadside pattern of f = 37.3 GHz also proves the unique OSB-free capability of the proposed CP LWA with fan-shaped slots. Moreover, the CP property can be switched between RHCP and LHCP modes at the broadside direction.

Fig. 11 presents the simulated ARs of the proposed CP LWA for two individual ports, which are all less than 3 dB for the corresponding main beams of the frequencies between 27.4 GHz - 37.3 GHz. As a result, the fractional CP bandwidth (BW) for ARs less than 3 dB is as wide as 31%.

Based on the above simulated results, we compared this design with other pol-flexible CP SIW LWAs [40]-[42] and collected their performances in Table I. As shown in Table I, this proposed SIW LWA has obvious advantages in terms of the compact final size, broad CP BW, wide beam steering range, and high gain.

IV. CONFORMAL CUBESAT ARRAY

In this section, the above designed single CP LWA is further developed into an array and applied into CubeSat communication system. Taking a 1U CubeSat as an applicable platform and the above CP LWA as an array element, a conformal high gain CubeSat SIW LWA array is proposed, optimized, and implemented in this section.

A. Vertical Coupling Feeding Method

According to the array scenario discussed in the Section II.A, the beam direction of an LWA needs to radiate at the −45-degrees, in order to achieve a sum beam in the $\hat{\boldsymbol{e}}_t$ direction. And the simulated results in the Section III.B indicate that the single LWA radiates at ±45 degrees at 28 GHz when the Port 1 or 2 are excited. So here we focus on the CP radiation of the array at 28 GHz, which is our designed operation center frequency. According to the parameter analysis in Section III, the optimal AR value in the −45-degrees direction corresponds to the following slot parameters: xc = −1 mm, dc =2.7 mm, t = 150 ° and xr = −0.4 mm.

Fig. 12 (a) shows the structure of the proposed conformal high gain LWA array on a 1U CubeSat. Two LWA elements, namely LWA 1 and LWA 2, are deployed perpendicularly at one corner of the CubeSat, which can be simultaneously excited by a well-designed vertical coupling feeding structure at the junction of these two LWAs. Fig. 12 (b) and (c) give the structures of LWA 1 and LWA 2, including both front and back views. As given in Fig. 12 (b), LWA 1 with a total length of 102 mm keeps the original two feeding ports, and two rectangular grooves, as the concave part of mortise-tenon joint, are made around the Port 2. LWA 2 with a total length of 95 mm, as shown in Fig. 12 (c), has one feeding port and two convex structures on the other end. By inserting the two convex structures into the concave parts of LWA 1, as illustrated in Fig. 12 (d), the two vertical LWAs are fixed together.

As analyzed in Part B of Section II, the two vertically arranged LWAs should be simultaneously excited by sources with equal amplitudes and 180 ° phase differences. Therefore, for the purpose of equally dividing input power of Port 1 into the two LWAs channels, we designed a coupling window on the ground of the LWA 1. Fig. 13 shows an optimization model for the transition design by a coupling window. As shown in Fig. 13 (a), for saving the simulation time, two short SIWs are adopted here, and connected through the middle coupling

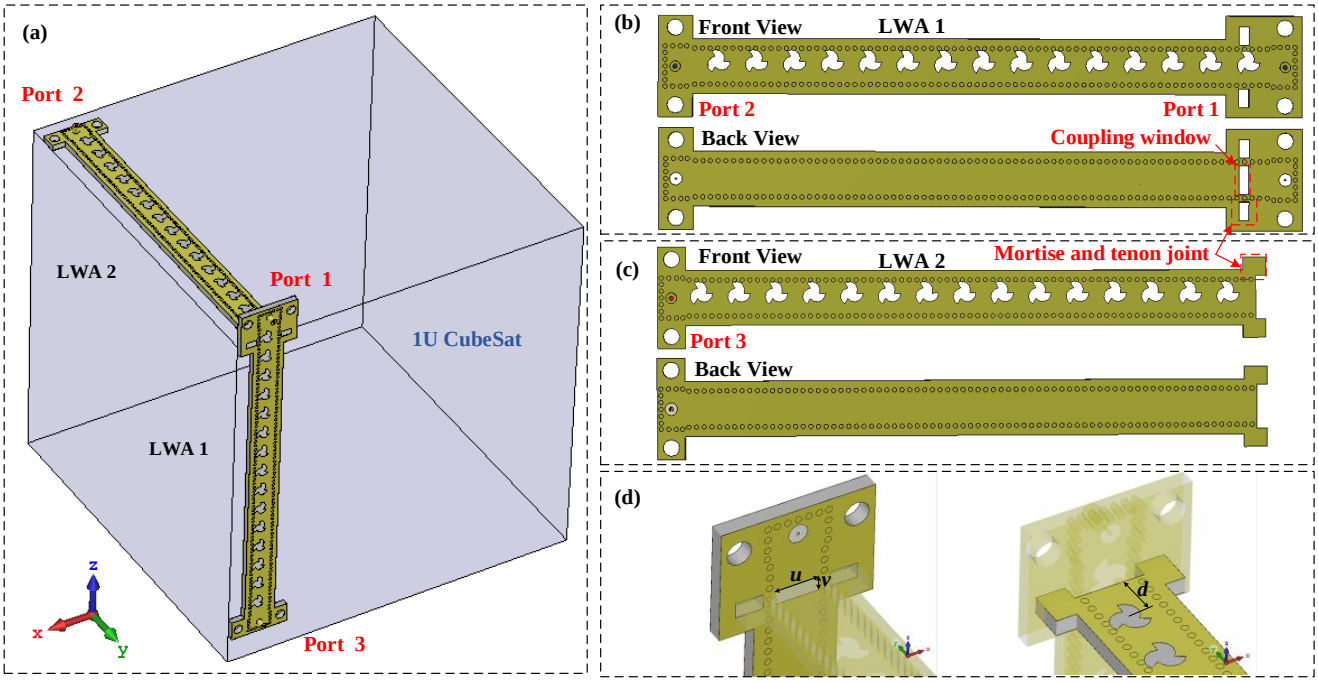

Fig. 12. Structure of the proposed conformal high gain CubeSat LWA array. (a) Configuration of the proposed array on 1 U CubeSat. (b) Front and back views of LWA 1. (c) Front and back views of LWA 2. (d) Vertical coupling feeding structure with mortise-tenon connection.

window on the ground of one SIW. In Fig. 13 (b), the vertical SIW's patch is taken off to show the coupling window clearly.

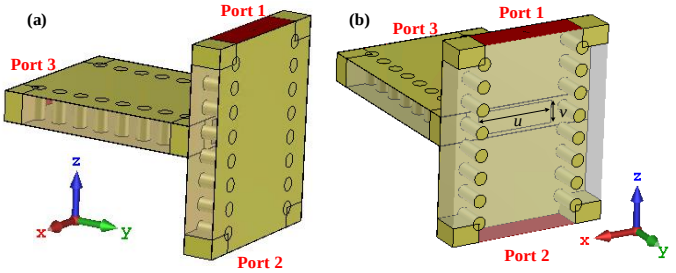

Fig. 13. Optimization model for coupling window design. (a) Configuration of the two SIW channels. (b) Dimensions of coupling window.

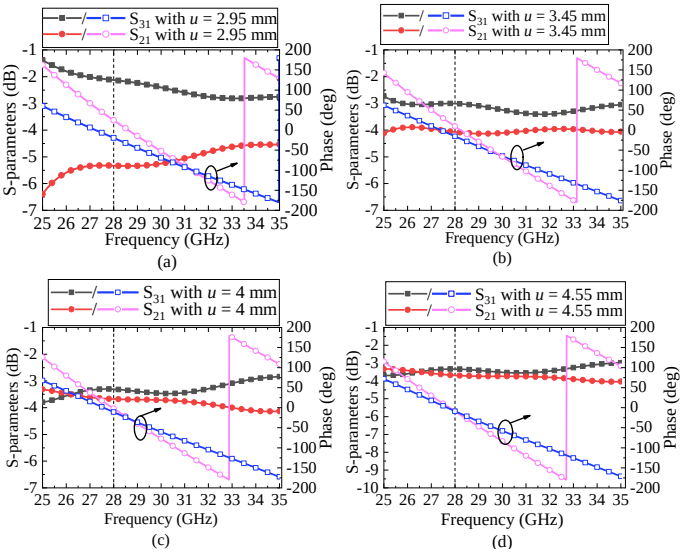

Fig. 14. Simulated S-parameters for the optimization of coupling window. (a) u = 2.95 mm. (b) u = 3.45 mm. (c) u =4 mm. (d) u = 4.55 mm.

In order to introduce as much energy as possible into the horizontal channel, the geometry center of coupling window is aligned to the center of the horizontally placed SIW channel.

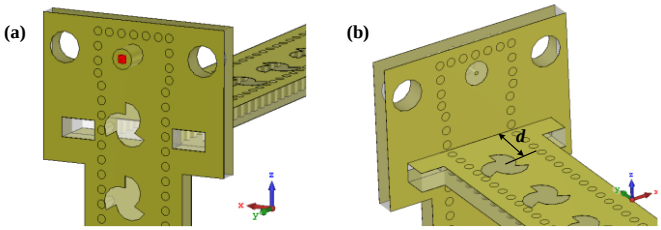

Fig. 15. Illustrations of vertical coupling feeding structure. (a) View of coupling window. (b) View of the first slot position.

The dimension of the coupling window is the key of deciding the power dividing ratio. Fig. 14 gives the optimization process of the window width u. As we can see from the S_{21} and S_{31}, when the window height v is fixed as 1.524 mm, S_{21} and S_{31} approach to be equal when u increases. When u is larger than 4 mm, the difference between than S_{21} and S_{31} becomes very small. It means the feeding energy of Port 1 can be more evenly distributed to the two SIW channels when the coupling window with a large size. Same optimization principles are also suitable for the selection of v, so v is set to the maximum possible value, namely 1.524 mm, which is the height of the substrate of SIW. With the selected u = 4.55 mm and v = 1.524 mm, the final achieved values of S_{21} and S_{31} are −3.6 dB and −3.3 dB respectively at 28 GHz, which means the power fed into the two SIWs are almost equal.

The 180 ° phase difference is realized by designing a path difference between the slot arrays in the two SIWs. Fig. 15 shows the details of the vertical coupling feeding structure. As shown in Fig. 15 (a), the first slot in the LWA 1 locates above

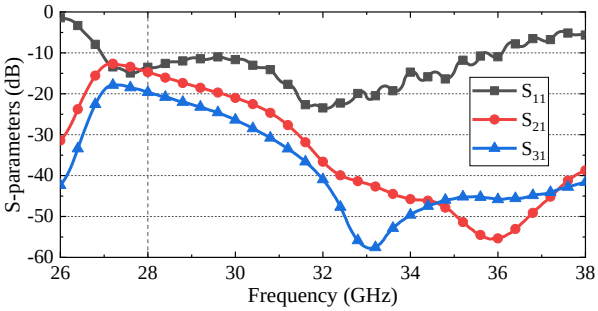

Fig. 16. Simulated S-parameters of the proposed CubeSat array.

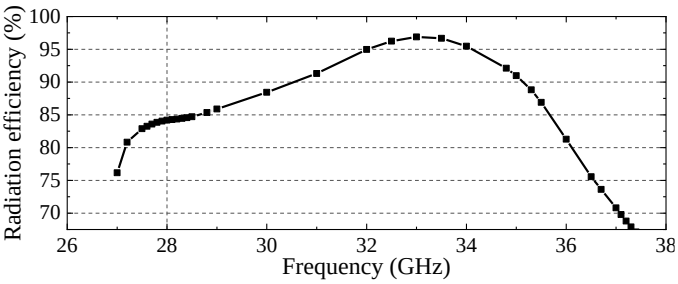

Fig. 17. Simulated radiation efficiency of the proposed CubeSat array.

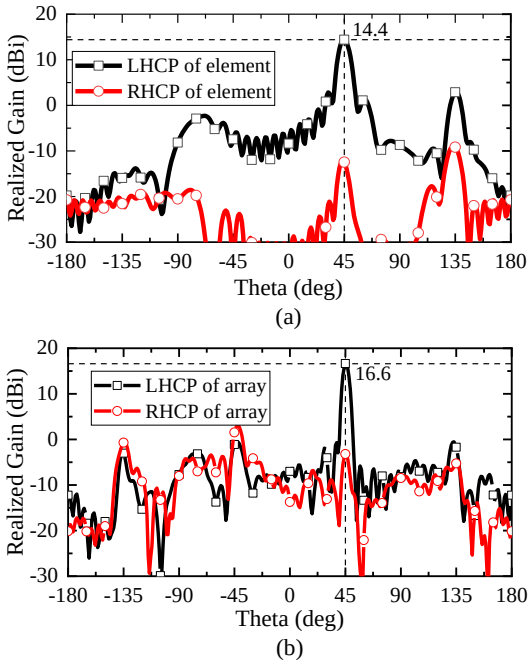

Fig. 18. Simulated radiation patterns of the proposed CubeSat array. (a) LWA element. (b) LWA array.

the coupling window. By controlling the distance *d* that is the distance between the first slot in the slot array of LWA 2 and the coupling window, the phase difference between two LWAs can be manipulated. To obtain a 180-degrees phase difference, *d* should be equal to the half waveguide wavelength in the SIW, i.e., 4.99 mm. In the optimization of the LWA array, taking the gain of sum as the goal, *d* is further tuned to be 4.7 mm.

B. Simulation Results of CubeSat Array

As shown in Fig. 12, when the Port 1 is excited, LWA 1 and LWA 2 in the proposed CubeSat array exhibits the LHCP radiation. Since their beams all point to −45-degrees direction

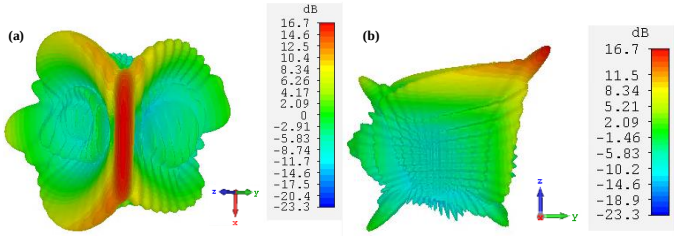

Fig. 19. Simulated 3D radiation patterns of the proposed CubeSat array. (a) Diagonal-line view. (b) Front View.

and can be effectively superposed, a high gain sum beam in the diagonal direction of the CubeSat can be expected. In this part, simulated results of this CubeSat array are presented and analysis.

Fig. 16 shows the simulated S-parameters of the proposed CubeSat array. As shown in Fig. 16, the S_{11} at the operation frequency of 28 GHz is −15.5 dB, and the S_{21} and S_{31} at 28 GHz are −12.5 dB and −17.2 dB respectively, which indicates the large leakage constant of the array consisting with two LWA elements. As shown in Fig. 17, the radiation efficiency at 28 GHz is 84.2%, indicating the high efficiency characteristic of the proposed array.

Fig. 18 gives the simulated radiation patterns of the CubeSat array and the corresponding LWA element (LWA 1 without coupling window). The realized co-pol gain of the conformal array is 16.6 dBi, while the co-pol gain of an array element is 14.4 dBi. The gain of the sum beam is 2.2 dBi higher than that of the sub beam, validating that the superposition of two sub patterns is effective. To visualize the pattern of sum beam, Fig. 19 provides 3D radiation patterns of the CubeSat array. It is seen that two sub patterns are well added in the main beam direction, and the sum beam correctly points to the diagonal direction. In addition, the cro-pol gains of the array and the array element are −3.2 dBi and −12.4 dBi. The side lobe level (SLL) of the array is −17.1 dB, and the SLL of the array element is −11.5 dB. Moreover, the 3 dB beamwidth of the array is 5.1 °, which shows high directivity feature than the element which has a 3 dB beamwidth of 9.1 °. The AR values of the array and the element are 1.8 dB and 0.8 dB, respectively. Therefore, the CubeSat array not only remains good LHCP property, but also realizes high gain and SLL reduction at the same time.

Since the beam direction varies with the operating frequencies for LWAs, the effective frequency bandwidth of the sum beam is also studied. Fig. 20 gives the simulated farfield patterns of the CubeSat array at 27.6 GHz, 27.8 GHz, 28.2 GHz and 28.4 GHz. As shown in Fig. 20, the simulated sum patterns at 27.8 GHz and 28.2 GHz still shows a good main beam shape while their gains are 16.4 dBi and 16 dBi (2 dBi and 1.6 dBi higher than the element). However, the sum patterns at 27.6 GHz and 28.4 GHz shows the lobe separation phenomenon and their gains decreases to 14.9 dBi and 14.4 dBi, respectively. Therefore, the effective frequency bandwidth of high gain CubeSat array is 27.8 GHz - 28.2 GHz.

V. Experiment And Results

For validating our proposed scenario and the aforementioned design and the simulated results, both the CP LWA element and

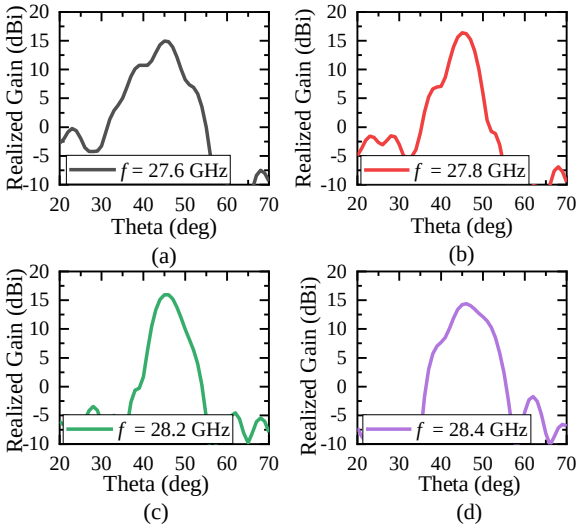

Fig. 20. Simulated radiation patterns of the proposed CubeSat array versus different frequencies. (a) 27.6 GHz. (b) 27.8 GHz. (c) 28.2 GHz. (d) 28.4 GHz.

Fig. 21. Phototype of the proposed CP LWA element.

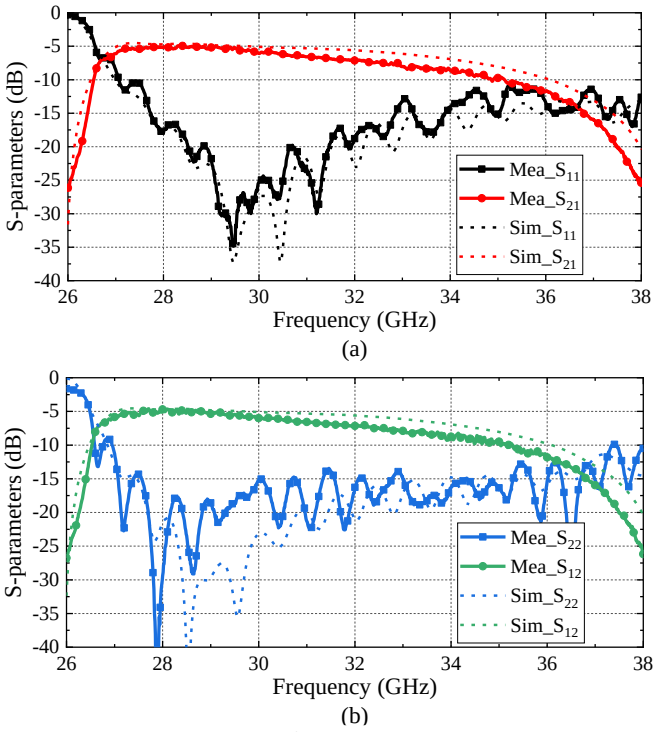

Fig. 22. Measured S-parameters of the proposed CP LWA element. (a) Port 1 mode. (b) Port 2 mode.

the CubeSat array are fabricated using printed circuit technology and tested in the laboratory.

A. Measured Results of Single CP LWA

The fabricated phototype of the proposed CP LWA is given in Fig. 21. The two ports of this element are excited respectively to obtain radiation results in two CP operation modes. When

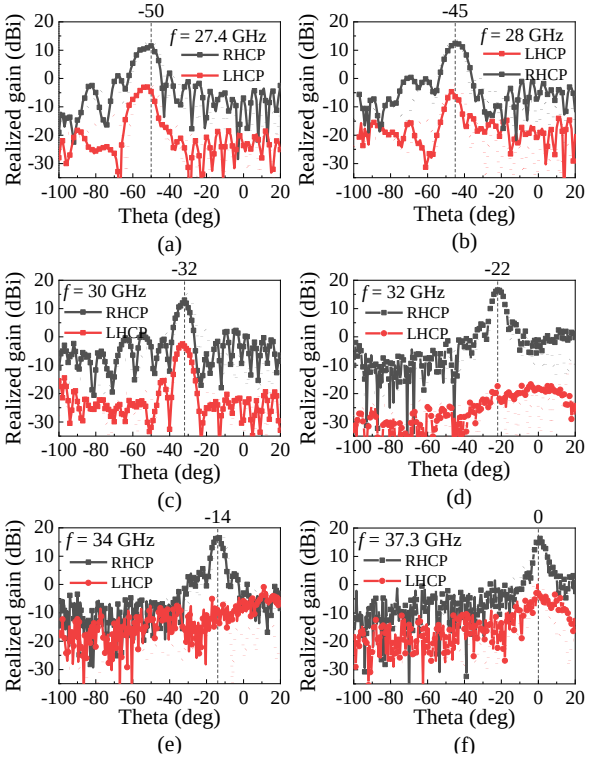

Fig. 23. Measured radiation patterns of the proposed CP LWA element when Port 1 is excited. (a) 27.4 GHz. (b) 28 GHz. (c) 30 GHz. (d) 32 GHz. (e) 34 GHz. (f) 37.3 GHz. (Dashed lines: simulated results.)

one port is used as the input port, the other port is connected to a 50 Ω matching load.

The measured S-parameters of the proposed CP LWA are plotted in Fig. 22, in which the simulated results are also given for comparison. Fig. 22 (a) gives the measured S-parameters when Port 1 is excited, in which the measured S_{11} and S_{21} has similar trends with the simulated results. The measured S_{11} values in the frequency band of 27.4 - 37.3 GHz are below −10 dB, whereas the measured S_{21} varies from −5 dB to −18.2 dB with the increase of frequencies. Similar results can also be observed in Fig. 22 (b) that illustrates measured S-parameters of Port 2 mode. We can see that no OSB exists in the broad frequency band of both Port 1 and Port 2 modes. However, the measured S_{21} values are lower than the simulated values in the high frequency region, which is caused by the insertion losses from extra connectors.

Fig. 23 and Fig. 24 show the measured radiation patterns of the CP LWA element. As shown in Fig. 23, the Port 1 mode realizes the continuous RHCP beam scanning in the backward directions ranging from −50 ° to 0 °, whereas the Port 2 mode obtains the continuous LHCP beam steering in the forward region from 0 °to 48 °in Fig. 24. Its realized gain and AR value with frequency basically have the same trends with the simulated results. Here, the measured results of the Port 1 mode are discussed and compared with its simulated results. Among them, the measured co-pol gains of the Port 1 mode at 27.4 GHz, 28 GHz, 30 GHz, 32 GHz, 34 GHz, and 37.3 GHz are 11.45 dBi, 11.38 dBi, 13.2 dBi, 15.45 dBi, 16.6 dBi and 16.4 dBi, which are 0.95 - 1.47 dBi lower than the simulated results. The measured gains of cro-pol patterns in the Port 1 mode are −4.6

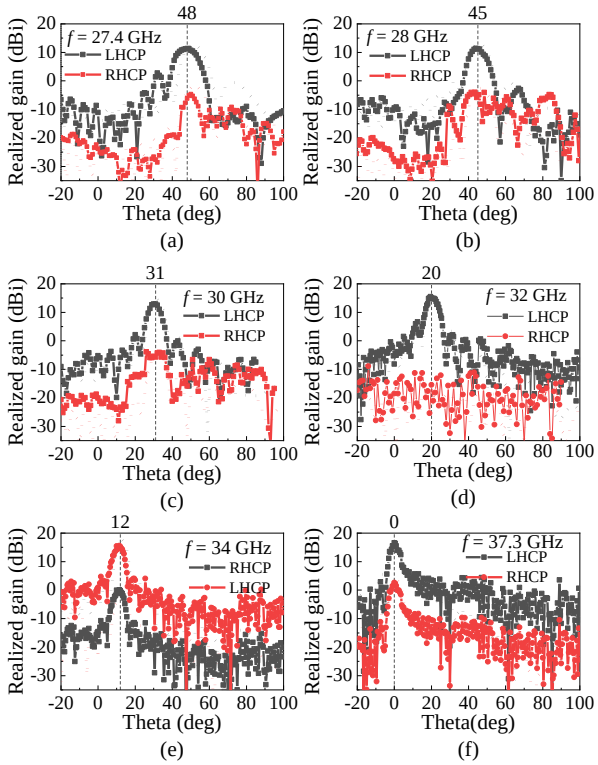

Fig. 24. Measured radiation patterns of the proposed CP LWA element when Port 2 is excited. (a) 27.4 GHz. (b) 28 GHz. (c) 30 GHz. (d) 32 GHz. (e) 34 GHz. (f) 37.3 GHz. (Dashed lines: simulated results.)

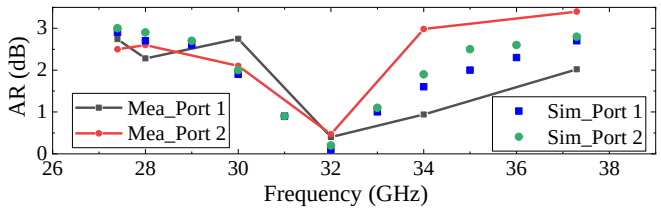

Fig. 25. Measured AR of the proposed CP LWA element

dBi, −6.3 dBi, −2.8 dBi, −17.4 dBi, −8.27 dBi and −2.3 dBi, respectively. According to the measured gain difference between the RHCP and LHCP patterns, the measured AR values of the above frequencies are 2.74 dB, 2.28 dB, 2.75 dB, 0.4 dB, 0.94 dB and 2.02 dB. Similar gain drop appears in the cro-pol gain curves, which is brought by measurement error of loading extra connector. The above discussion is also applicable to the Port 2 mode. The measured co-pol/cro-pol gains of the Port 2 mode at 27.4 - 37.3 GHz are 11.3/-5.5 dBi, 11.37/-5.1 dBi, 12.9/-5.3 dBi, 15.7/-15.5 dBi, 15.7/0.4 dBi and 16.98/2.92 dBi. According to above results, the measured AR values can be calculated as 2.5 dB, 2.6 dB, 2.1 dB, 0.47 dB, 2.98 dB and 3.4 dB, which is plotted in Fig. 25. Through above analysis, the characteristic of wide CP band and pol-flexible function of the proposed LWA design are validated.

B. Measured Results of CubeSat Array

The fabricated phototype of the proposed CP LWA is given in Fig. 26. Here, a cube box with a side length of 10 cm is taken to represent the 1U CubeSat, and the fabricated array is placed on one corner of the cube to illustrate its conformal structure. In the measurement, the middle port of this element is fed with

Fig. 26. Phototype of the proposed CubeSat array.

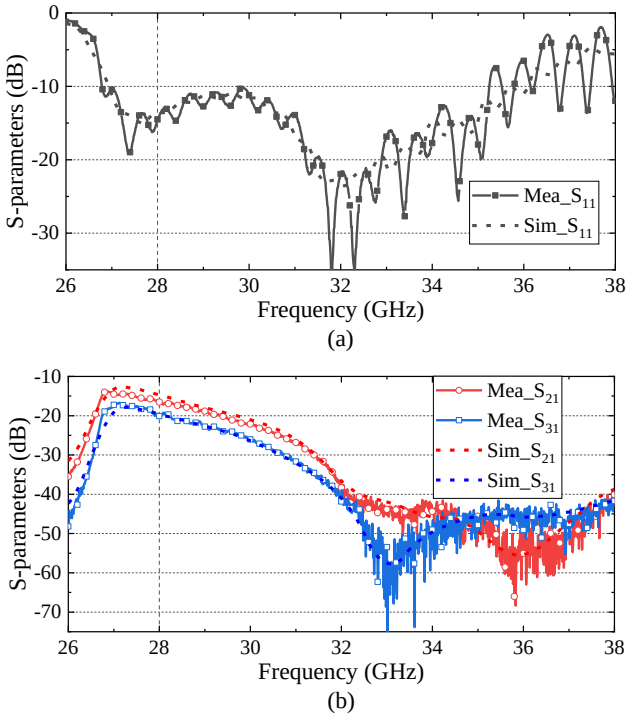

Fig. 27. Measured S-parameters of the proposed CubeSat array. (a) S_{11}. (b) S_{21} and S_{31}.

a coaxial connector, the other two ports are connected to 50 Ω matching loads.

The measured S-parameters of the proposed CubeSat array are given in Fig. 27. As shown in Fig. 27 (a), the measured S_{11} at the operating frequency 28 GHz is below −10 dB, which agrees well with the simulated results. As shown in Fig. 27 (b), the measured S_{21} and S_{31} at 28 GHz are −16.6 dB and −20 dB respectively, which also shows a similar trend with the simulated curves.

Fig. 28 shows the measured radiation patterns of the conformal CubeSat array. As shown in Fig. 28, the sum beam points at 45 degrees with a high co-pol gain of 15.7 dBi. The measured co-pol gain is −5.6 dBi, and the measured AR is calculated to be 1.5 dB. The measured gain difference between LHCP and RHCP patterns is 20.3 dB, showing a good polarization purity. Among them, the measured co-pol and cro-pol gains are 0.9 dB and 3.4 dB less than the simulated ones. The above differences are still within the allowable range, which mainly caused by experiment errors.

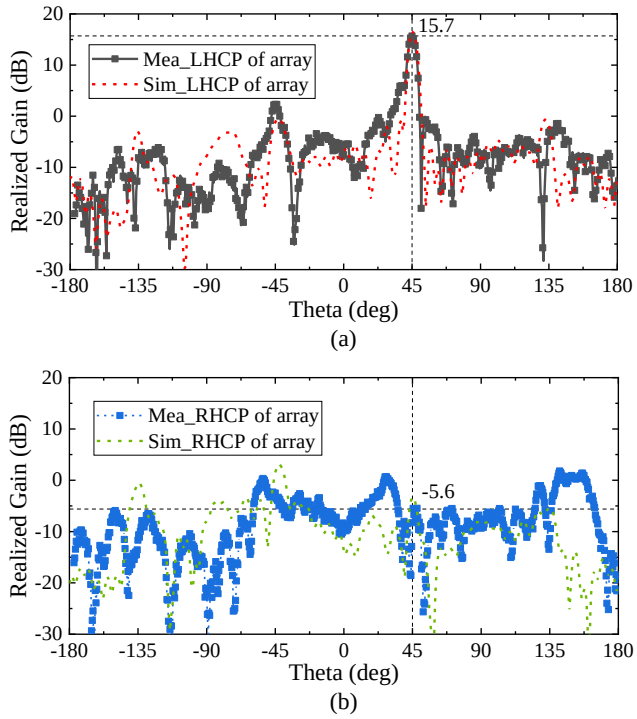

Fig. 28. Measured radiation patterns of the proposed CubeSat array at 28 GHz. (a) LHCP. (b) RHCP.

VI. Conclusion

From a forward-looking perspective of small satellite communication, like CubeSat communication, planar antennas with flexible features of circular polarization and beam scanning are necessary and preferred. This paper promotes the study of CP LWAs in the aspect of switchable polarization and free of open stopband. Based on the outstanding element design, a conformal high gain LWA array with two vertically arranged units for a 1U CubeSat is carried out. With the proposed superposition of sub patterns, we can further achieve a longitudinally foldable LWA with suitable length for 3U, 6U or 12 U communications. Moreover, the radiation efficiency and realized gain of the LWA array has been greatly raised in this scenario.

VII. Acknowledgment

The authors would like to thank Cristian Alistarh and Grant Gourley of the Heriot-Watt University for their assistance and support in antenna measurement in the anechoic chamber.

References

[1] K. Woellert, P. Ehrenfreund, A. J. Ricco, and H. Hertzfeld, "Cubesats: Cost-effective science and technology platforms for emerging and developing nations," *Adv. Space Res.*, vol. 47, no. 4, pp. 663–684, 2011.

[2] N. E. Chahat, "A mighty antenna from a tiny cubesat grows," *IEEE Spectr.*, vol. 55, no. 2, pp. 32–37, February 2018.

[3] N. Chahat, E. Decrossas, D. Gonzalez-Ovejero, O. Yurduseven, M. J. Radway, R. E. Hodges, P. Estabrook, J. D. Baker, D. J. Bell, T. A. Cwik, and G. Chattopadhyay, "Advanced cubesat antennas for deep space and earth science missions: A review," *IEEE Antennas Propag. Mag.*, vol. 61, no. 5, pp. 37–46, Oct 2019.

[4] N. Chahat, R. E. Hodges, J. Sauder, M. Thomson, E. Peral, and Y. Rahmat-Samii, "Cubesat deployable ka-band mesh reflector antenna development for earth science missions," *IEEE Trans. Antennas Propag.*, vol. 64, no. 6, pp. 2083–2093, June 2016.

[5] J.-K. Che, C.-C. Chen, J. T. Johnson, E. Kraus, D. Laczkowski, M. A. Solly, and K. Horgan, "6 ghz to 40 ghz cubesat radiometer antenna system," *IEEE Trans. Antennas Propag.*, vol. 67, no. 5, pp. 3410–3415, 2019.

[6] Y. Rahmat-Samii, V. Manohar, J. M. Kovitz, R. E. Hodges, G. Freebury, and E. Peral, "Development of highly constrained 1 m ka-band mesh deployable offset reflector antenna for next generation cubesat radars," *IEEE Trans. Antennas Propag.*, vol. 67, no. 10, pp. 6254–6266, 2019.

[7] J. Costantine, Y. Tawk, I. Maqueda, M. Sakovsky, G. Olson, S. Pellegrino, and C. G. Christodoulou, "Uhf deployable helical antennas for cubesats," *IEEE Trans. Antennas Propag.*, vol. 64, no. 9, pp. 3752–3759, Sep. 2016.

[8] M. Hwang, G. Kim, S. Kim, and N. S. Jeong, "Origami-inspired radiation pattern and shape reconfigurable dipole array antenna at c-band for cubesat applications," *IEEE Trans. Antennas Propag.*, vol. 69, no. 5, pp. 2697–2705, 2021.

[9] J. Costantine, Y. Tawk, C. G. Christodoulou, J. Banik, and S. Lane, "Cubesat deployable antenna using bistable composite tape-springs," *IEEE Antennas Wireless Propag. Lett.*, vol. 11, pp. 285–288, 2012.

[10] T. F. C. Leao, V. Mooney-Chopin, C. W. Trueman, and S. Gleason, "Design and implementation of a diplexer and a dual-band vhf/uhf antenna for nanosatellites," *IEEE Antennas Wireless Propag. Lett.*, vol. 12, pp. 1098–1101, 2013.

[11] R. E. Hodges, N. Chahat, D. J. Hoppe, and J. D. Vacchione, "A deployable high-gain antenna bound for mars: Developing a new folded-panel reflectarray for the first cubesat mission to mars." *IEEE Antennas Propag. Mag.*, vol. 59, no. 2, pp. 39–49, 2017.

[12] Y. Tawk, "Physically controlled cubesat antennas with an adaptive frequency operation," *IEEE Antennas Wireless Propag. Lett.*, vol. 18, no. 9, pp. 1892–1896, 2019.

[13] A. D. Johnson, V. Manohar, S. B. Venkatakrishnan, and J. L. Volakis, "Low-cost s-band reconfigurable monopole/patch antenna for cubesats," *IEEE Open Journal of Antennas and Propagation*, vol. 1, pp. 598–603, 2020.

[14] R. Fdhila, T. M. Hamdani, and A. M. Alimi, "A multi objective particles swarm optimization algorithm for solving the routing pico-satellites problem," in *Proc. IEEE Int. Conf. Syst.*, Man, Cybern., 2012, pp. 1402–1407.

[15] P. Puig-suari, C. Turner, and R. Twiggs, "Cubesat: The development and launch support infrastructure for eighteen different satellite customers on one launch," in *Proc. 15th Annu. USU Conf. Small Satellites*, 01 2001, pp. 1–5.

[16] C. J. Vourch and T. D. Drysdale, "V-band "bull's eye" antenna for cubesat applications," *IEEE Antennas Wireless Propag. Lett.*, vol. 13, pp. 1092–1095, 2014.

[17] A. Nascetti, E. Pittella, P. Teofilatto, and S. Pisa, "High-gain s-band patch antenna system for earth-observation cubesat satellites," *IEEE Antennas Wireless Propag. Lett.*, vol. 14, pp. 434–437, 2015.

[18] X. Liu, D. R. Jackson, J. Chen, J. Liu, P. W. Fink, G. Y. Lin, and N. Neveu, "Transparent and nontransparent microstrip antennas on a cubesat: Novel low-profile antennas for cubesats improve mission reliability." *IEEE Antennas Propag. Mag.*, vol. 59, no. 2, pp. 59–68, 2017.

[19] M. Samsuzzaman, M. T. Islam, S. Kibria, and M. Cho, "Birds-1 cubesat constellation using compact uhf patch antenna," *IEEE Access*, vol. 6, pp. 54 282–54 294, 2018.

[20] T. R. Jones, J. P. Grey, and M. Daneshmand, "Solar panel integrated circular polarized aperture-coupled patch antenna for cubesat applications," *IEEE Antennas Wireless Propag. Lett.*, vol. 17, no. 10, pp. 1895–1899, 2018.

[21] M. J. Veljovic and A. K. Skrivervik, "Aperture-coupled low-profile wideband patch antennas for cubesat," *IEEE Trans. Antennas Propag.*, vol. 67, no. 5, pp. 3439–3444, 2019.

[22] S. Liu, R. Raad, P. I. Theoharis, and F. Tubbal, "Dual-band folded-end dipole antenna for plastic cubesats," *IEEE Journal on Miniaturization for Air and Space Systems*, vol. 1, no. 3, pp. 172–178, 2020.

[23] A. Narbudowicz, R. Borowiec, and S. Chalermwisutkul, "No-need-to-deploy UHF antenna for cubesat: Design based on characteristic modes," *IEEE Antennas Wireless Propag. Lett.*, vol. 20, no. 4, pp. 508–512, 2021.

[24] P. Bouc¸a, J. N. Matos, S. R. Cunha, and N. B. Carvalho, "Low-profile aperture-coupled patch antenna array for CubeSat applications," *IEEE Access*, vol. 8, pp. 20 473–20 479, 2020.

[25] J. Wang, Y. Geng, C. Zhang and X. Huo, "Radiation characteristic of the periodic leaky wave structure and its application to leaky wave antenna design," 2015 *Asia-Pacific Microwave Conference (APMC)*, Nanjing, 2015.
[26] X. Li, J. Wang, Z. Li, Y. Li, M. Chen and Z. Zhang, "Dual-Beam Leaky-Wave Antenna Array With Capability of Fixed-Frequency Beam Switching," *IEEE Access*, vol. 8, pp. 28155-28163, 2020.
[27] X. Li, J. Wang, Z. Li, Y. Li, Y. Geng, M. Chen and Z. Zhang, " Leaky-wave Antenna Arrays for Flexible Dual-beam Switching," *IEEE Trans. Antennas Propag*, Early access, 2021.
[28] M. M. Sabahi, A. A. Heidari and M. Movahhedi, "A Compact CRLH Circularly Polarized Leaky-Wave Antenna Based on Substrate-Integrated Waveguide," in *IEEE Trans. Antennas Propag.*, vol. 66, no. 9, pp. 4407-4414, Sept. 2018.
[29] W. Getsinger, "Elliptically polarized leaky-wave array," *IRE Trans. Antennas Propag.*, vol. 10, no. 2, pp. 165–171, 1962.
[30] H. Lee, J. H. Choi, C.-T. M. Wu, and T. Itoh, "A compact single radiator crlh-inspired circularly polarized leaky-wave antenna based on substrate-integrated waveguide," *IEEE Trans. Antennas Propag.*, vol. 63, no. 10, pp. 4566–4572, 2015.
[31] P. Chen, W. Hong, Z. Kuai, and J. Xu, "A substrate integrated waveguide circular polarized slot radiator and its linear array," *IEEE Antennas Wireless Propag. Lett*., vol. 8, pp. 120–123, 2009.
[32] C. Liu, Z. Li, and J. Wang, "A new kind of circularly polarized leaky-wave antenna based on corrugated substrate integrated waveguide," in *Proc. IEEE 5th Int. Symp. Microw., Antenna, Propag. EMC Technol. Wireless Commun. (MAPE)*, 2013, pp. 383–387.
[33] G. Mishra, S. K. Sharma and J. -C. S. Chieh, "A High Gain Series-Fed Circularly Polarized Traveling-Wave Antenna at W-Band Using a New Butterfly Radiating Element," *IEEE Trans. Antennas Propag.*, vol. 68, no. 12, pp. 7947-7957, Dec. 2020.
[34] S. Chen, D. K. Karmokar, P. Qin, R. W. Ziolkowski and Y. J. Guo, "Polarization-Reconfigurable Leaky-Wave Antenna With Continuous Beam Scanning Through Broadside," *IEEE Trans. Antennas Propag.*, vol. 68, no. 1, pp. 121-133, Jan. 2020.
[35] F. Wu, R. Lu, J. Wang, Z. H. Jiang, W. Hong and K. -M. Luk, "A Circularly Polarized 1 Bit Electronically Reconfigurable Reflectarray Based on Electromagnetic Element Rotation," in *IEEE Trans. Antennas Propag.*, vol. 69, no. 9, pp. 5585-5595, Sept. 2021.
[36] S.-L. Chen, D. K. Karmokar, Z. Li, P.-Y. Qin, R. W. Ziolkowski, and Y. J. Guo, "Circular-polarized substrate-integrated-waveguide leaky-wave antenna with wide-angle and consistent-gain continuous beam scanning," *IEEE Trans. Antennas Propag.*, vol. 67, no. 7, pp. 4418–4428, 2019.
[37] J. Liu, X. Tang, Y. Li, and Y. Long, "Substrate integrated waveguide leaky-wave antenna with h-shaped slots," *IEEE Trans. Antennas Propag.*, vol. 60, no. 8, pp. 3962–3967, 2012.
[38] A. Suntives and S. V. Hum, "A fixed-frequency beam-steerable halfmode substrate integrated waveguide leaky-wave antenna," *IEEE Trans. Antennas Propag.*, vol. 60, no. 5, pp. 2540–2544, May 2012.
[39] H. Lee, J. H. Choi, Y. Kasahara, and T. Itoh, "A circularly polarized single radiator leaky-wave antenna based on crlh-inspired substrate in-tegrated waveguide," in *IEEE MTT-S Int. Microw. Symp. Dig.(IMS2014)*, 2014, pp. 1–3.
[40] A. Pourghorban Saghati, M. M. Mirsalehi and M. H. Neshati, "A HMSIW Circularly Polarized Leaky-Wave Antenna With Backward, Broadside, and Forward Radiation," in *IEEE Antennas Wireless Propag. Lett.*, vol. 13, pp. 451-454, 2014.
[41] J. Zhong, A. K. Rashid and Q. Zhang, "45 ° Linearly Polarized and Circularly Polarized High-Scanning-Rate Leaky-Wave Antennas Based on Slotted Substrate Integrated Waveguide," in *IEEE Access*, vol. 8, pp. 82162-82172, 2020.
[42] Y. J. Cheng, W. Hong, and K. Wu, "Millimeter-wave half mode substrate integrated waveguide frequency scanning antenna with quadri-polarization," *IEEE Trans. Antennas Propag.*, vol. 58, no. 6, pp. 1848–1855, 2010.
[43] Y. Dong and T. Itoh, "Substrate integrated composite right-/left-handed leaky-wave structure for polarization-flexible antenna application," *IEEE Trans. Antennas Propag.*, vol. 60, no. 2, pp. 760–771, 2012.
[44] A. Sarkar, S. Mukherjee, A. Sharma, A. Biswas and M. Jaleel Akhtar, "SIW-Based Quad-Beam Leaky-Wave Antenna With Polarization Diversity for Four-Quadrant Scanning Applications," *IEEE Trans. Antennas Propag.*, vol. 66, no. 8, pp. 3918-3925, Aug. 2018.

Xiaowen Li was born in Shandong, China, in 1992. She is received the B.E. degree from the School of Opto-Electronic Information Science and Technology, Yantai University, China in 2015. Since 2016, She has been studying for the Ph.D. degree in the Institute of Lightwave Technology, Beijing Jiaotong University. From 2020, she is a visiting student with the Microwaves and Antenna Engineering Group, Heriot-Watt university, Edinburgh, UK.
Her research fields are leaky-wave antennas and array for flexible beam scanning.

Junhong Wang (M'02–SM'03) was born in Jiangsu, China, in 1965. He received the B.S. and M.S. degrees in electrical engineering from the University of Electronic Science and Technology of China, Chengdu, China, in 1988 and 1991, respectively, and the Ph.D. degree in electrical engineering from Southwest Jiaotong University, Chengdu, China, in 1994. In 1995, he joined as the Faculty with the Department of Electrical Engineering, Beijing Jiaotong University, Beijing, China, where he became a Professor in 1999. From January 1999 to June 2000, he was a Research Associate with the Department of Electric Engineering, City University of Hong Kong, Kowloon Tong, Hong Kong. From July 2002 to July 2003, he was a Research Scientist with Temasek Laboratories, National University of Singapore, Singapore. He is currently with the Key Laboratory of all Optical Network and Advanced Telecommunication Network, Ministry of Education of China, Beijing Jiaotong Univeristy, Beijing, China, and also with the Institute of Lightwave Technology, Beijing Jiaotong University, Beijing, China. His research interests include numerical methods, antennas, scattering, and leaky wave structures.

George Goussetis (S 99, M 02, SM 12) received the Diploma degree in Electrical and Computer Engineering from the National Technical University of Athens, Greece, in 1998, and the Ph.D. degree from the University of Westminster, London, UK, in 2002. In 2002 he also graduated B.Sc. in physics (first class) from University College London (UCL), UK.
In 1998, he joined the Space Engineering, Rome, Italy, as RF Engineer and in 1999 the Wireless Communications Research Group, University of Westminster, UK, as a Research Assistant. Between 2002 and 2006 he was a Senior Research Fellow at Loughborough University, UK. He was Assistant Professor with Heriot-Watt University, Edinburgh, UK between 2006 and 2009 and Associate Professor with Queen's University Belfast, UK, between 2009 and 2013. In 2013 he joined Heriot-Watt and was promoted to

Professor in 2014. He currently directs the Institute of Sensors Signals and Systems at Heriot-Watt University. He has authored or co-authored over 500 peer-reviewed papers five book chapters one book and five patents. His research interests are in the area of microwave and antenna components and subsystems.

Dr. Goussetis held research fellowships from the Onassis foundation in 2001, the UK Royal Academy of Engineering between 2006-2011, and European Commission Marie-Curie in 2011-12 and again in 2014-17. He is the co-recipient of the 2011 European Space Agency young engineer of the year prize, the 2011 EuCAP best student paper prize, the 2012 EuCAP best antenna theory paper prize and the 2016 Bell Labs prize. He served as Associate Editor to the IEEE Antennas and Wireless Propagation Letters between 2014-18.

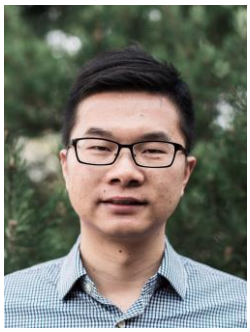

Lei Wang (S'09-M'16-SM'19) received the Ph.D. degree in electromagnetic field and microwave technology from the Southeast University, Nanjing, China in 2015. From 2014 to 2016, he was a Research Fellow and Postdoc in the Laboratory of Electromagnetics and Antennas, Swiss Federal Institute of Technology (EPFL) in Lausanne, Switzerland. From 2016 to 2017, he was a Postdoc in Electromagnetic Engineering Laboratory of KTH Royal Institute of Technology in Stockholm, Sweden. From 2017 to 2020, he was an Alexander von Humboldt fellow in the Institute of Electromagnetic Theory of Hamburg University of Technology (TUHH) in Hamburg, Germany. From March 2020 to present, he is an Assistant Professor in the Institute of Signals, Sensors and Systems of Heriot-Watt University in Edinburgh, United Kingdom. His research includes the antenna theory and applications, active electronically scanning arrays, integrated antennas and arrays, substrate-integrated waveguide antennas, leaky-wave antennas, and wireless propagations.

He was awarded the Chinese National Scholarship for PhD Candidates in 2014 and was granted the Swiss Government Excellence Scholarship to conduct research at EPFL in 2014 too. He was also granted the Alexander von Humboldt fellowship to carry out research at TUHH in 2016. Moreover, he received the Best Poster Award in 2018 IEEE International Workshop on Antenna Technology (iWAT) and the Best Paper Award in the 5th International Conference on the UK-China Emerging Technologies (UCET2020).